Electron paramagnetic resonance studies of nitrogen interstitial defects in diamond

2009 J. Phys.: Condens. Matter 21 364212

(http://iopscience.iop.org/0953-8984/21/36/364212)

J. Phys.: Condens. Matter **21** (2009) 364212 (8pp) doi:10.1088/0953-8984/21/36/364212

Electron paramagnetic resonance studies of nitrogen interstitial defects in diamond

S Felton[1], B L Cann[1], A M Edmonds[1], S Liggins[1], R J Cruddace[1], M E Newton[1], D Fisher[2] and J M Baker[3]

[1] Department of Physics, University of Warwick, Coventry CV4 7AL, UK
[2] Diamond Trading Company, DTC Research Centre, Belmont Road, Maidenhead, Berkshire SL6 6JW, UK
[3] Oxford Physics, Clarendon Laboratory, Oxford OX1 3PU, UK

E-mail: m.e.newton@warwick.ac.uk

Received 1 April 2009
Published 19 August 2009
Online at stacks.iop.org/JPhysCM/21/364212

Abstract

We report on electron paramagnetic resonance (EPR) studies of nitrogen doped diamond that has been ^{15}N enriched, electron irradiated and annealed. EPR spectra from two new nitrogen containing $S = \frac{1}{2}$ defects are detected and labelled WAR9 and WAR10. We show that the properties of these defects are consistent with them being the ⟨001⟩-nitrogen split interstitial and the ⟨001⟩-nitrogen split interstitial–⟨001⟩-carbon split interstitial pair, respectively. We also provide an explanation for why these defects have previously eluded discovery.

1. Introduction

Isolated vacancies and self-interstitials are produced by the irradiation of diamond with particles of sufficient energy to displace carbon atoms. The production of primary and secondary irradiation damage defects has been intensively studied in intrinsic diamond. The neutral (V^0) and negatively (V^-) charged isolated vacancy have been thoroughly characterized by optical [1–5] and EPR spectroscopy [6, 7], and experiment and theory are in good accord. The activation energy for migration of V^0 is 2.2 eV [8], and in intrinsic diamond substantial concentrations of di-vacancies can be produced by annealing at 1100 K [9]. There is no evidence for excitation enhanced migration of the vacancy [10], however the situation is far more complicated for the interstitial. Theoretically the ⟨001⟩-split-self-interstitial (I_{001}) is by far the lowest energy configuration [11], and this is the only one observed and characterized by EPR [10] and optical spectroscopy [12]. For 1–2 MeV electron irradiation at ∼100 K the production of isolated vacancies and interstitials is identical [10]. However as the temperature is increased excitation enhanced migration of the interstitial with an activation energy of ∼0.3 eV has been observed [13]. It is uncertain as to whether this enhanced mobility is due to electronic excitation of the neutral I_{001} defect or is characteristic of e.g. I^-_{001}. This result explains the production of di-interstitial aggregates upon room temperature irradiation [14], whereas post-irradiation annealing shows that the activation energy for migration of I_{001} is 1.6 eV [13, 15]. Following annealing above the migration temperature of I_{001} a three interstitial aggregate has been observed by EPR [16] and a diamagnetic four interstitial aggregate predicted by theory [11].

Nitrogen is a common impurity in both natural and synthetic diamond and it is used as the basis for classifying diamond [17]: Type I diamond contains significant quantities of nitrogen as measured by Infra-red (IR) absorption; Type II diamond does not. Type I diamond is further subdivided into Type Ia, in which the nitrogen is present in aggregated forms, and Type Ib, containing mostly single substitutional nitrogen, N_S. Common forms of aggregated nitrogen in diamond are two nearest neighbour substitutional nitrogen atoms, known as the A-centre, four substitutional nitrogen atoms surrounding a vacant lattice site (vacancy), called the B-centre, and three substitutional nitrogen atoms next to a vacancy, labelled N3 [17].

Much is known of the interaction of vacancies with nitrogen impurities. Charge transfer from the neutral single substitutional nitrogen (N^0_S) donor produces V^-

$$V^0 + N^0_S \rightleftarrows V^- + N^+_S.$$

Upon annealing above ∼900 K the stationary N_S readily traps vacancies to produce nitrogen vacancy complexes

$$N^0_S + V \rightarrow NV^0$$

$$NV^0 + N_S^0 \rightarrow NV^- + N_S^+$$

and both the neutral and negatively charged NV centres are discussed extensively elsewhere [8, 18, 19]. Substitutional nitrogen pairs (A-centres) also trap mobile vacancies (although less efficiently than N_S) to produce N–V–N defects [8]; again neutral (H3) and negatively charged (H2) versions are produced [20–23]. The NV centre anneals out at ∼1800 K, with the associated production of A-centres via vacancy-assisted aggregation

$$NV + N_S \rightarrow N_S\text{–}N_S + V$$

$$N_S + V \rightarrow NV$$

etc

[24]. High temperature annealing (under stabilizing pressures) of nitrogen containing diamond usually results in specimens with detectable (at least by photoluminescence) concentrations of $NV^{0/-}$ and $NVN^{0/-}$, which have been 'quenched' in, but this will not be discussed further here [23, 25].

Our understanding of the fate of interstitials in nitrogen doped diamond is far less advanced. We know that (R1) di-interstitials are not produced in diamond doped with N_S when the concentration of nitrogen greatly exceeds that of the interstitials produced by irradiation damage [26]. The production of isolated I_{001}^0 interstitials was not altered by the presence of N_S^0 [26], indicating that even with the deep donor present the neutral charge state of I_{001} is preferred. Once mobile we postulate that the I_{001} interstitials are trapped by N_S^0 producing N_I

$$I_{001} + N_S^0 \rightarrow N_I$$

where one of the atoms of the interstitial dumbbell is replaced by the nitrogen atom. It is unlikely that N_I would dissociate but migrate as a unit [27], once mobile. Goss *et al* [27] predicted that the barrier to migration for N_I^- is substantially less than that for N_I^0. The capture of I_{001} by N_I would produce an R1 like di-interstitial with one of the three-fold coordinated carbons replaced with a nitrogen ($[N_I\text{–}I_{001}]$). Capture of N_I by N_S would produce N_{2I} where both dumbbell atoms of the interstitial are replaced by nitrogens. Goss *et al* [27] proposed that this defect was responsible for the H1a local vibrational mode [28]. In the neutral charge state both N_I and $N_I\text{–}I_{001}$ would be paramagnetic and should be observable by EPR if not obscured by other defects; the detection of both is the subject of this paper.

We can postulate further that in diamond where the nitrogen is incorporated as A-centres mobile interstitials will be trapped by A-centres to produce N_{2I} directly. Indeed this was the argument put forward by Goss *et al* to explain the different temperatures at which H1a is annealed into type Ib and type Ia diamond [27].

It has been shown that incorporation of nitrogen in HPHT diamond is growth sector dependent, with {111} sectors typically showing the highest N_S concentration [29]. Burns *et al* [29] found that in a sample where the {111} sectors contained ∼100 ppm (atomic parts per million) N_S^0 the {100} sectors contained ∼50 ppm N_S^0 with the {113} and {110} sectors containing substantially less N_S^0 at ∼10 ppm and ∼1 ppm, respectively. Thus following irradiation, it is important to bear in mind that we have to consider both the situations where $[N_S^0] \gg [V], [I_{001}]$ and $[N_S^0] \ll [V], [I_{001}]$ in a mixed growth sector sample. In the former we are likely to produce diamagnetic N_I^- and $[N_I\text{–}I_{001}]^-$, in the latter paramagnetic N_I^0 and $[N_I\text{–}I_{001}]^0$ when interstitials are mobile. Following the work by Goss *et al* [27] on the mobilities of N_I^0 and N_I^- we might expect different concentrations of the defects in the different growth sectors. We have to consider carefully the consequences of different mobilities and stabilities in the two charge states.

2. Experimental details

The sample used in this study is a synthetic mixed type IaA/Ib diamond. It was grown using a modified high pressure, high temperature (HPHT) synthesis method [30]: atmospheric gases were removed from the growth capsule containing the solvent/catalyst and carbon source by heating it in vacuum. At a lower temperature, the removed gases were replaced with ^{15}N enriched gases. The growth capsule was then sealed and the pre-treated reaction mixture was subjected to HPHT conditions in the diamond stable region. This produced a type Ib sample, where >95% of the nitrogen was ^{15}N, with a mean bulk concentration of approximately 150 ppm N_S^0 [30]. The sample is made up of several different growth sectors. Through HPHT annealing >80% of the N_S in the high concentration sectors was aggregated to A-centres, making these sectors mixed type IaA, with an A-centre concentration of ∼60 ppm and an N_S^0 concentration of ∼30 ppm. In the sectors with low nitrogen concentration, little or no aggregation is likely to have occurred: if we assume that the low nitrogen sectors have a concentration of 1 ppm N_S^0 annealing at a temperature of 2300 K would only yield a 1% aggregation to A-centres, while the same annealing temperature would lead to ∼80% aggregation to A-centres in sectors with 150 ppm N_S^0 [31, 32]. After the HPHT annealing the sample was irradiated with 1.5 MeV e^- to a dose of 4×10^{17} electrons cm^{-2} at room temperature leading to a vacancy (V^0 and V^-) concentration of ∼3 ppm [10]. The mean bulk concentration of V^- was determined from the EPR spectra recorded post-irradiation, figure 1(b), to be ∼1 ppm. The sample was subsequently annealed for 4 h at 1100 K in an non-oxidising atmosphere, to create secondary irradiation defects such as NV centres and possibly nitrogen interstitial defects such as N_I, N_{2I} etc. The annealing time and temperature were chosen to remove all isolated vacancies [8].

Room temperature EPR spectra for the sample were collected using a Bruker EMX continuous wave X-band spectrometer with an operating frequency of ∼9.75 GHz and a custom-built Q-band spectrometer, which has been described elsewhere by Twitchen *et al* [14]. An Oxford Instruments Liquid Helium ESR900 flow cryostat was used with the Bruker EMX X-band spectrometer to perform measurements at cryogenic temperatures.

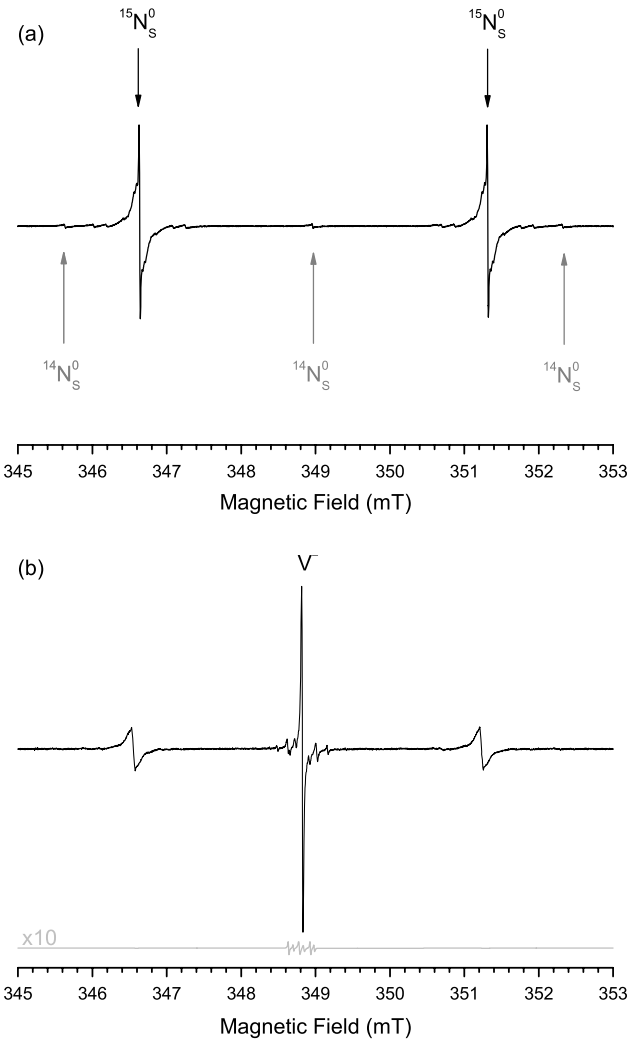

Figure 1. X-band first derivative EPR spectra (black line) recorded with the magnetic field applied along ⟨001⟩ for the sample (a) post-HPHT treatment but pre-irradiation and (b) post-irradiation. Note that the $^{15}N_S^0$ EPR spectrum, marked with black arrows in (a), is made up of components with different line widths due to variation in concentrations of defects in different sectors of the sample. The much less intense lines of the $^{14}N_S^0$ EPR spectrum are marked with grey arrows in (a). In (b) note the large signal, with ^{13}C satellites, in the middle of the spectrum from the negatively charged vacancies present in the sample post-irradiation. For comparison, simulated spectra of the two new defects (grey line) are shown below the experimental spectrum, at approximately ten times the signal intensity expected from the concentration detected post-annealing. The vertical scale in (a) is half that of (b). Note that the narrow component of the N_S^0 EPR spectrum is dramatically diminished in (b) compared to (a). This is attributed to almost complete charge transfer from N_S to V in the low nitrogen sectors, see text for details.

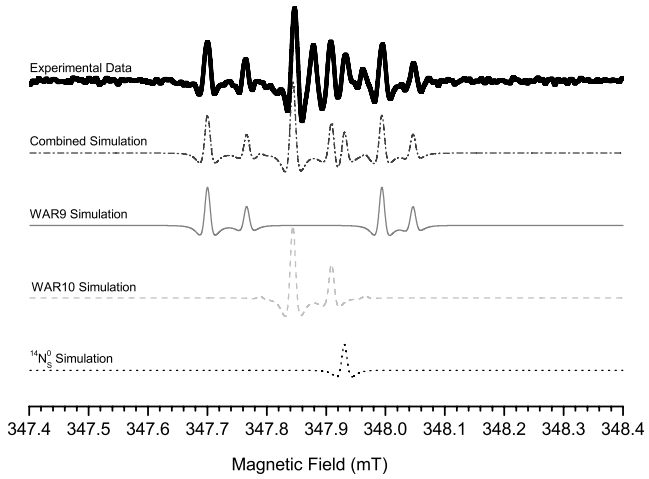

Figure 2. X-band second derivative experimental (thick black line) and simulated spectra at $f = 9.752$ GHz with the magnetic field applied along ⟨001⟩. The solid grey line (——) shows the simulated WAR9 spectrum, the dashed grey line (- - - -) shows the simulated WAR10 spectrum, and the dotted black line (· · · · · ·) shows the $^{14}N_S^0$ spectrum. This line is used as a g-marker and the electronic Zeeman parameters of table 1 are referenced to the g-value 2.0024 of N_S^0 [34]. The grey dash–dotted line (— · —) shows the sum of all the simulated spectra.

The presence of sectors with different defect concentrations in the sample is confirmed by the EPR spectra, see e.g. figure 1(a), where it can be clearly seen that the N_S^0 EPR spectrum is made up of signals with components of different line widths [33]. For a nitrogen defect concentration of the order of 10 ppm or above the EPR line width increases roughly linearly with the defect concentration; for concentrations below 10 ppm the line width is determined by the interaction with the ^{13}C present at natural abundance of 1.1% in the sample [33]. From this we can conclude that there are regions in the studied sample with defect concentrations below 10 ppm and other regions with defect concentrations up to an order of magnitude larger. As discussed in section 1 the {110} sectors may contain as little as 1 ppm of N_S^0. Consequently there is likely to have been regions of the sample where the vacancy concentration was roughly equal to the concentration of N_S. If $[N_S^0] \leqslant [V]$ in the low nitrogen sectors $V^0 + N_S^0 \rightarrow V^- + N_S^+$ so that in these sectors almost all of the N_S is present as diamagnetic N_S^+. This assumption is supported by figure 1(b), where the narrow component of the N_S^0 EPR spectrum is dramatically reduced compared to figure 1(a).

Figure 1(b) shows an EPR spectrum of the sample post-irradiation, where the large signal in the centre of the spectrum is from the negatively charged vacancy [6]. This is the region of the spectrum where the lines from the new defects appear, so that even if they were present in the sample post-irradiation but pre-annealing, they would not be detectable due to overlap with the negative vacancy signal.

3. Results

EPR measurements post-irradiation and annealing revealed spectra from two previously unreported defects, labelled WAR9 and WAR10, each showing hyperfine interaction with one ∼100% abundant $I = \frac{1}{2}$ nucleus, see figures 2 and 3. The EPR spectra for the new defects both have line widths of 0.02 mT, like the narrow component of the N_S^0 spectrum. From the integrated intensity of the EPR signal of the WAR9 and WAR10 spectra the mean bulk concentration of these defects were found to be 0.10(1) ppm (atomic parts

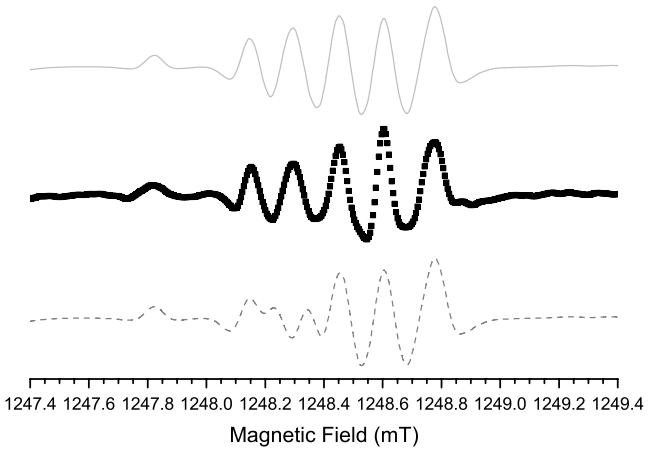

Figure 3. Q-band second derivative experimental (■) and simulated spectra at $f = 35$ GHz for WAR9, WAR10 and $^{14}N_S^0$ with the magnetic field applied along ⟨111⟩. The upper solid grey line (——) shows a simulation using the WAR10 parameters from table 1 and the lower dashed grey line (- - - -) shows a simulation using a spin Hamiltonian with lower g-symmetry and no hyperfine interaction for WAR10, which fits the X-band data. The parameters for WAR9 and $^{14}N_S^0$ are the same for both simulations. Only the simulation including a hyperfine interaction for WAR10 yields a satisfactory fit to the experimental data.

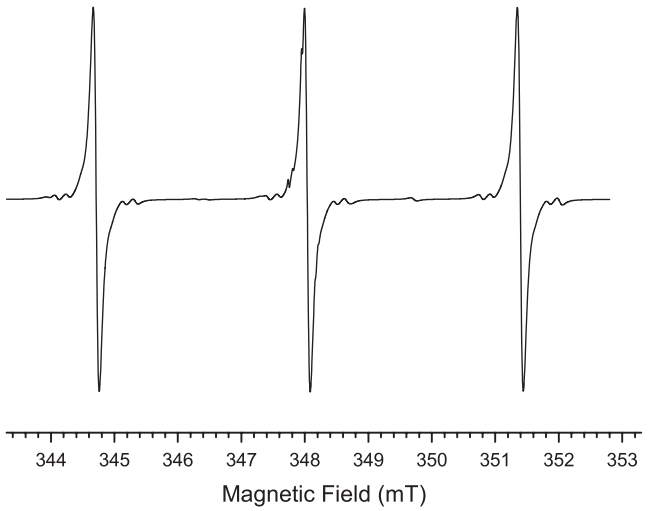

Figure 4. Simulated X-band first derivative EPR spectrum with the magnetic field applied along ⟨001⟩ showing $^{14}N_S^0$ overlapping with ^{14}N versions of WAR9 and WAR10. These have been simulated with the ^{15}N hyperfine interaction multiplied by the ratio of the nuclear Zeeman values for ^{14}N and ^{15}N [35]. The quadrupole interaction is set to zero.

per million) each. In the same way the $^{15}N_S^0$ and $^{14}N_S^0$ mean bulk concentrations were determined to be 20(2) ppm and 0.72(7) ppm, respectively. The sample also contains 0.6(1) ppm of NV^-.

X-band EPR roadmaps for the new defects were produced by recording spectra with the magnetic field applied at 5°

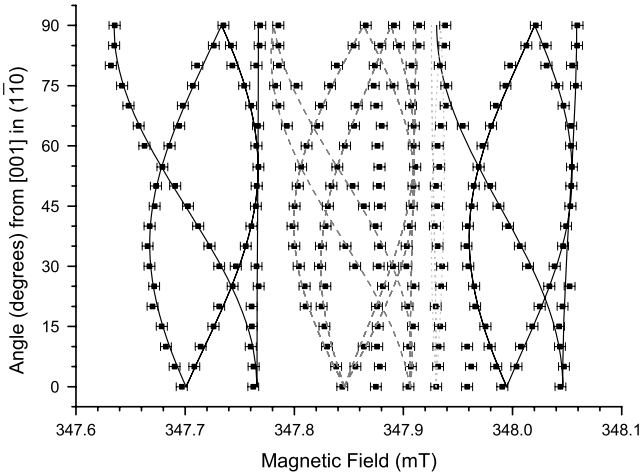

Figure 5. X-band EPR line positions for different orientations of the applied magnetic field in the crystallographic (1$\bar{1}$0) plane. The points (■) represent experimental peak positions and the lines show simulated peak positions for WAR9 as solid lines (——) and WAR10 as dashed lines (- - - -) using the fitted parameters of table 1. The dotted line (· · · · · ·) shows the position of the central $^{14}N_S^0$ peak, see also figure 2.

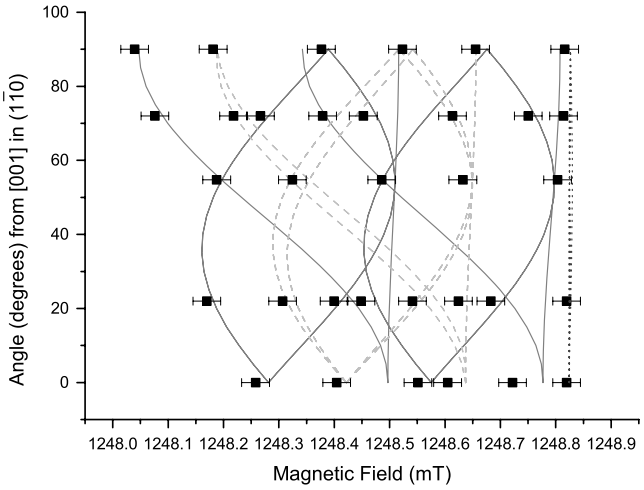

Figure 6. Q-band EPR line positions for different orientations of the applied magnetic field in the crystallographic (1$\bar{1}$0) plane. The points (■) represent experimental peak positions and the lines show simulated peak positions for WAR9 as solid lines (——) and WAR10 as dashed lines (- - - -) using the fitted parameters of table 1. The dotted line (· · · · · ·) shows the position of the central $^{14}N_S^0$ peak.

increments in a {110} crystallographic plane, see figure 5. Q-band EPR spectra were recorded with the magnetic field applied along the three principal directions ⟨001⟩, ⟨110⟩ and ⟨111⟩, as well as two intermediate directions in a {110} plane, see figure 6. The orientation of the applied magnetic field, **B**, with respect to the crystallographic directions was determined from the position of the $^{15}N_S^0$ EPR lines.

In a ^{14}N doped sample the central transition of the N_S^0 EPR spectrum with its associated satellites appears in the same field range as the entire WAR9 and WAR10 spectra. Figure 4 shows a simulated EPR spectrum with the magnetic field applied parallel to ⟨001⟩ from approximately 20 ppm of $^{14}N_S^0$ overlaid

Table 1. Spin Hamiltonian parameters for the two new ^{15}N containing defects with directions $[\theta, \varphi]$, where θ is the angle from the crystallographic [001] direction and φ is the angle from [100] measured towards [010] in the (100) plane.

Defect	g_1	g_2	g_3
WAR9	2.003 43(10) ∥ [90°, 45°]	2.002 72(10) ∥ [180°, 45°]	2.002 68(10) ∥ [90°, 315°]
WAR10	2.003 44(10) ∥ [90.1(2)°, 45.0(2)°]	2.002 72(10) ∥ [179.9(2)°, 45.0(2)°]	2.002 69(10) ∥ [90°, 315°]
	A_1 (MHz)	A_2 (MHz)	A_3 (MHz)
WAR9	8.30(5) ∥ [90°, 45°]	7.85(5) ∥ [180°, 45°]	8.17(5) ∥ [90°, 315°]
WAR10	1.00(4) ∥ [44.8(3)°, 45.0(7)°]	−1.01(4) ∥ [134.8(3)°, 45.0(7)°]	0.00(4) ∥ [90°, 315°]

on a simulation of the detected concentration of WAR9 and WAR10 but with the hyperfine interaction scaled with the ratio of nuclear Zeeman values for ^{14}N and ^{15}N [35]. As can be clearly seen in this figure, the WAR9 and WAR10 signals are almost impossible to separate from the $^{14}N_S^0$ EPR spectrum, illustrating the importance of isotopical substitution of nitrogen for the detection of these two defects. The WAR9 and WAR10 lines are centred around $g \approx 2.002$ and all found within a 0.5 mT range of fields at X-band and 1.0 mT at Q-band as can be seen in figures 5 and 6.

No change in the EPR spectrum for WAR9 and WAR10 was detected down to the lowest measured temperature of 10 K. The intensities of the WAR9 and WAR10 EPR signals have not been found to change on annealing the sample up to a temperature of 1800 K.

4. Analysis of the data

The X-band EPR spectra from the two new defects were fitted to the spin Hamiltonian

$$H = \mu_B \mathbf{B} \cdot \underline{\mathbf{g}} \cdot \mathbf{S} + \mathbf{S} \cdot \underline{\mathbf{A}} \cdot \mathbf{I} - g_N \mu_N \mathbf{B} \cdot \mathbf{I} \qquad (1)$$

with an electronic spin $S = \frac{1}{2}$ and nuclear spin $I = \frac{1}{2}$ from a ^{15}N nucleus, varying the electronic Zeeman interaction, $\underline{\mathbf{g}}$, and the hyperfine interaction, $\underline{\mathbf{A}}$, see table 1. The WAR9 defect was constrained to have orthorhombic C_{2v} symmetry and the WAR10 defect was constrained to have a {110} mirror plane. Removing these constraints did not significantly improve the quality of fit. The parameters yield an excellent fit to the experimental data for all magnetic field directions for both the X- and Q-band measurements, as can be seen in figures 2, 5 and 6. The lines in the X-band spectra at ∼347.93 mT, for all orientations of the magnetic field, are due to the central transition of the $^{14}N_S^0$ spectrum. This line was used as a g-marker and the determined electronic Zeeman parameters are referenced to its literature g-value of 2.0024(5) [34].

It is possible to achieve an equally good fit to the experimental WAR10 line positions at X-band using a spin Hamiltonian with only an electronic Zeeman interaction with C_{1h} symmetry keeping only the {110} mirror plane. However, this does not yield a satisfactory fit to the Q-band data. This is illustrated in figure 3 which shows the experimental Q-band spectrum recorded with the magnetic field parallel to ⟨111⟩ together with two different simulated spectra: the top one is simulated using the spin Hamiltonian parameters of table 1 and the bottom one using the parameters obtained when fitting the X-band WAR10 line positions assuming C_{1h} symmetry and only an anisotropic electronic Zeeman interaction. Only the simulation involving a hyperfine interaction with ^{15}N fits both the Q-band and X-band data, see also figure 2. The hyperfine interaction is assumed to be with a ^{15}N nucleus for both WAR9 and WAR10 since this is the only ∼100% abundant $I = \frac{1}{2}$ nucleus in this sample.

5. Discussion

As can be seen in table 1 the two new defects have identical electronic Zeeman parameters, with orthorhombic symmetry and a ⟨110⟩ C_{2v} symmetry axis. The hyperfine interactions, on the other hand, are very different. For WAR9 the hyperfine interaction has the same ⟨110⟩ C_{2v} symmetry axis as the electronic Zeeman interaction and small anisotropy, while the hyperfine interaction in WAR10 has an isotropic component that is approximately zero and the symmetry is lowered to C_{1h}, keeping the {110} mirror plane.

The WAR9 and WAR10 EPR spectra are detected after electron irradiation and annealing to 1100 K. However, since the EPR signal from negatively charged isolated vacancies [6] appears in the same region of the spectrum as WAR9 and WAR10, see figure 1(b), these defects would not be detected until the vacancies have been annealed out. There are therefore several possibilities for when the WAR9 and WAR10 defects are formed. The centres could be formed directly after the irradiation, which could provide an explanation for the fact that in samples containing N_S no R1 is formed on electron irradiation [26]: WAR9 and WAR10 are formed instead. Another possibility is that WAR9 and WAR10 are formed after annealing at some temperature <1100 K, the annealing temperature used in this study. For example, the isolated, neutral ⟨001⟩-split-self-interstitial (I_{001}) giving rise to the R2 EPR spectrum is stable up to 700 K [10, 36]. The WAR9 and WAR10 defects could be formed as I_{001} becomes mobile. It is of course also possible that these defects are only formed at the temperature the sample was annealed at. They would in any case not be detectable before the V^- EPR signal has disappeared from the spectrum.

5.1. Model for WAR9

For the ⟨001⟩-split nitrogen interstitial, N_I, illustrated in figure 7(b), we expect C_{2v} symmetry and inclusion of one nitrogen atom and that it is formed after irradiation and possibly annealing. This defect should be EPR active with

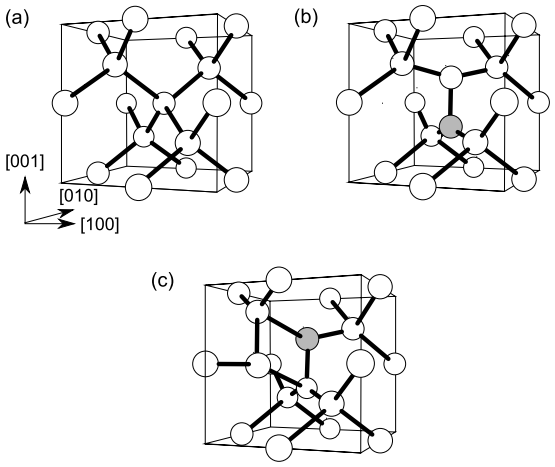

Figure 7. Models of the diamond lattice adapted from the paper by Goss *et al* [11]. The unfilled circles are carbon atoms and the filled circles are nitrogen atoms. (a) shows the undistorted diamond lattice, (b) shows a ⟨100⟩-split nitrogen interstitial, N_I, and (c) shows a nitrogen interstitial–self-interstitial pair, N_I–I_{001}.

$S = \frac{1}{2}$ in the neutral charge state. The ⟨001⟩-split nitrogen interstitial model is an analogue of the $(N–B)_i^+$ defect which gives rise to the EPR spectrum labelled NIRIM-4 [37]. In this centre the majority of the unpaired electron density is localized on the nitrogen atom with a minor amount on the boron; for N_I we expect to have a filled p_π orbital on the nitrogen atom and a half-filled p_π orbital on the carbon atom, so that the majority of the unpaired electron probability density is localized on the carbon atom. Scaling the magnitude of the ^{11}B hyperfine interaction for NIRIM-4 [37] with the ratio of the ^{11}B to ^{15}N nuclear Zeeman values [35], we get $|A_1| = 13.5$ MHz, $|A_2| = 10.4$ MHz and $|A_3| = 7.9$ MHz. The WAR9 defect has the required C_{2v} symmetry and the right $S = \frac{1}{2}$ spin to be the neutral charge state of N_I. The measured ^{15}N hyperfine values for WAR9 of approximately 8 MHz, see table 1, are also in reasonable agreement with those calculated from comparison with the NIRIM-4 centre. N_I^0 is therefore a possible model for the WAR9 defect.

If the N_S^0 is sufficiently high, the N_I may accept an electron from N_S^0 and become diamagnetic. The WAR9 spectrum has a narrow line width meaning that the signal comes from the low N_S regions of the sample. In the high N_S sectors we expect N_I to be in the negative charge state, which would be diamagnetic (as well as being in a region of the sample which has broader EPR lines). If Goss *et al*'s [27] model of the H1a IR centre [28] as a di-nitrogen interstitial, N_{2I}, is correct its likely formation mechanism in Type Ib diamond is trapping of N_I by N_S. Since H1a is formed on annealing at 950 K in Type Ib material, this suggests that the nitrogen interstitial is mobile at this temperature in the negative charge state. The neutral charge state of N_I may have a much higher thermal stability so that this does not rule out the assignment of WAR9 to N_I.

5.2. Model for WAR10

For a nearest neighbour ⟨001⟩-split nitrogen interstitial–self-interstitial pair, N_I–I_{001}, see figure 7(c), in the neutral charge state we expect, as for N_I, a filled p_π orbital on the nitrogen atom and a half-filled p_π orbital on the three-fold coordinated carbon atom, yielding a defect with C_{1h} symmetry and an $S = \frac{1}{2}$ ground state.

If we view the N_I–I_{001} defect as analogous to the R1 EPR centre it is possible to estimate the hyperfine interaction from a simple dipole–dipole calculation between the unpaired electron probability density and the nitrogen nucleus. The inter-radical distance of the R1 centre has been calculated to be 1.7 Å [11], so we set this to be the distance between the N-atom and the C-atom with the partially filled p_π orbital. From the ^{13}C hyperfine interaction in the R1 centre it has been estimated that approximately 70% of the unpaired electron probability density is in the partially filled p_π orbitals. Following Hunt *et al* [10] we therefore assume 35% of the unpaired electron probability density to be centred a distance X = 0.6 Å on either side of the C-nucleus along the $[1\bar{1}0]$ direction. This yields two contributions to the hyperfine interaction which were transformed to a common coordinate axes system and summed. The principal values of this hyperfine tensor are $A_1 = 1.6$ MHz, $A_2 = -1.0$ MHz and $A_3 = -0.6$ MHz with A_3 parallel to $[1\bar{1}0]$. Assuming that 0.4% of the unpaired electron probability density is localized on the N-atom yields an additional uniaxial hyperfine contribution of the form $A_\parallel = -2b$ and $A_\perp = b$ with $b = -0.3$ MHz and $A_\parallel$ along $[1\bar{1}0]$. Adding this to the hyperfine tensor from the electron dipole calculation results in a calculated hyperfine tensor with $A_1 = -A_2 = 1.3$ MHz and $A_3 = 0$ MHz, with A_3 still parallel to $[1\bar{1}0]$. This is the form and magnitude of the experimentally determined hyperfine interaction for WAR10, which also has the required $S = \frac{1}{2}$ spin state. The numerical values in the hyperfine calculation are very sensitive to the angle of the interaction, which is determined by the assumed C–N distance and position of the unpaired electron probability density along the p_π-orbital. The good numerical agreement between the calculated and experimental hyperfine interaction should therefore be viewed as fortuitous, but this calculation shows that a N_I–I_{001} model in the neutral charge state for WAR10 is consistent with the form of the hyperfine interaction.

As for WAR9 the narrow EPR line width for WAR10 shows that it is only present in the low N_S sectors. If N_I–I_{001} were present in the high N_S sectors it probably would not be detectable since in these regions it would be in the negative charge state and therefore diamagnetic. Since N_I^- is mobile below the temperatures the sample has been annealed at N_I–I_{001} may not be present in the high N_S sectors at all.

6. Conclusions

We have discovered two new nitrogen containing EPR active defects in irradiated and annealed diamond, which we label WAR9 and WAR10. We demonstrate that the formation of these defects after electron irradiation and annealing and their spin Hamiltonian parameters are consistent with them being the ⟨001⟩-nitrogen split interstitial (N_I) and the N_I–⟨001⟩ carbon interstitial pair (N_I–I_{001}), respectively, both in the neutral charge state. The use of an isotopically enriched sample, where >95% of the nitrogen was of the ^{15}N isotope, was the key to detecting these defects, since their EPR spectra

overlap with the central transition of the $^{14}N_S^0$ EPR spectrum. The narrow line widths of WAR9 and WAR10 indicate that they are only present in the low nitrogen regions of the sample, suggesting that both N_I and N_I–I_{001} are electron acceptors and exist in the negative charge state in the presence of N_S. This also means that even though the average bulk concentration of WAR9 and WAR10 is only ∼0.1 ppm, they are important irradiation products in low nitrogen sectors of diamond, which may only account for a fraction of the whole sample. The assignment of WAR9 and WAR10 to N_I and N_I–I_{001}, requires that both are stable to at least 1800 K. Other annealing data suggests that N_I^- is much more mobile and has not survived annealing to 1800 K. The difference in mobility of N_I^0 and N_I^- was suggested by theory [27]. Nevertheless at first sight the survival of N_I^0 and $[N_I–I_{001}]^0$ is surprising. However, in the low nitrogen sectors N_I^0 may be mobile but not able to find a trap at 1800 K.

Further work is required on both the annealing of N_I^0 and $[N_I–I_{001}]^0$, as well as determining the fraction of nitrogen which can be tied up in interstitial complexes; our results suggest that they are not necessarily minor players and should be considered when using ion implantation to produce useful colour centres in diamond (e.g. NV^-).

Acknowledgment

The authors thank Dr Joh Hansen of E6 Ltd for the synthesis of the sample.

References

[1] Davies G and Lightowlers E C 1970 Symmetry properties of ND1 absorption centre in electron-irradiated diamond *J. Phys. C: Solid State Phys.* **3** 638–50
[2] Clark C D and Walker J 1973 The neutral vacancy in diamond *Proc. R. Soc.* A **334** 241–57
[3] Davies G and Penchina C M 1974 Effect of uniaxial stress on GR1 doublet in diamond *Proc. R. Soc.* A **338** 359–74
[4] Davies G 1977 Charge states of vacancy in diamond *Nature* **269** 498–500
[5] Davies G and Foy C 1980 Jahn–Teller coupling at the neutral vacancy in diamond *J. Phys. C: Solid State Phys.* **13** 2203–13
[6] Isoya J, Kanda H, Uchida Y, Lawson S C, Yamasaki S, Itoh H and Morita Y 1992 EPR identification of the negatively charged vacancy in diamond *Phys. Rev.* B **45** 1436
[7] van Wyk J A, Tucker O D, Newton M E, Baker J M, Woods G S and Spear P 1995 Magnetic-resonance measurements on the $^5A_2$ excited-state of the neutral vacancy in diamond *Phys. Rev.* B **52** 12657–67
[8] Davies G, Lawson S C, Collins A T, Mainwood A and Sharp S J 1992 Vacancy-related centers in diamond *Phys. Rev.* B **46** 13157
[9] Twitchen D J, Newton M E, Baker J M, Banholzer W F and Anthony T 1999 Optical spin polarization in the di-⟨001⟩-split interstitial (R1) centre in diamond *Diamond Relat. Mater.* **8** 1101–6
[10] Hunt D C, Twitchen D J, Newton M E, Baker J M, Anthony T R, Banholzer W F and Vagarali S S 2000 Identification of the neutral carbon ⟨100⟩-split interstitial in diamond *Phys. Rev.* B **61** 3863
[11] Goss J P, Coomer B J, Jones R, Shaw T D, Briddon P R, Rayson M and Öberg S 2001 Self-interstitial aggregation in diamond *Phys. Rev.* B **63** 195208
[12] Davies G, Smith H and Kanda H 2000 Self-interstitial in diamond *Phys. Rev.* B **62** 1528–31
[13] Newton M E, Campbell B A, Twitchen D J, Baker J M and Anthony T R 2002 Recombination-enhanced diffusion of self-interstitial atoms and vacancy-interstitial recombination in diamond *Diamond Relat. Mater.* **11** 618–22
[14] Twitchen D J, Newton M E, Baker J M, Tucker O D, Anthony T R and Banholzer W F 1996 Electron-paramagnetic-resonance measurements on the di-⟨001⟩-split interstitial center (R1) in diamond *Phys. Rev.* B **54** 6988–98
[15] Allers L, Collins A T and Hiscock J 1998 The annealing of interstitial-related optical centres in type II natural and CVD diamond *Diamond Relat. Mater.* **7** 228–32
[16] Hunt D C, Twitchen D J, Newton M E, Baker J M, Kirui J K, van Wyk J A, Anthony T R and Banholzer W F 2000 EPR data on the self-interstitial complex O3 in diamond *Phys. Rev.* B **62** 6587
[17] Kiflawi I and Lawson S C 2001 Aggregates of nitrogen in diamond *The Properties, Growth and Application of Diamond* (*EMIS Datareview Series* vol 26) ed M H Nazare and A J Neves (London: INSPEC, the Institution of Electrical Engineers) pp 130–3
[18] Felton S, Edmonds A M, Newton M E, Martineau P M, Fisher D and Twitchen D J 2008 Electron paramagnetic resonance studies of the neutral nitrogen vacancy in diamond *Phys. Rev.* B **77** 081201(R)
[19] Felton S, Edmonds A M, Newton M E, Martineau P M, Fisher D, Twitchen D J and Baker J M 2009 Hyperfine interaction in the ground state of the negatively charged nitrogen vacancy center in diamond *Phys. Rev.* B **79** 075203–8
[20] Lawson S C, Davies G, Collins A T and Mainwood A 1992 The H2 optical-transition in diamond—the effects of uniaxial-stress perturbations, temperature and isotopic-substitution *J. Phys.: Condens. Matter* **4** 3439–52
[21] Mita Y, Nisida Y, Suito K, Onodera A and Yazu S 1990 Photochromism of H2 and H3 centers in synthetic type Ib diamonds *J. Phys.: Condens. Matter* **2** 8567–74
[22] Collins A T 1999 Things we still do not know about optical centres in diamond *Diamond Relat. Mater.* **8** 1455–62
[23] Collins A T, Connor A, Ly C H, Shareef A and Spear P M 2005 High-temperature annealing of optical centers in type-I diamond *J. Appl. Phys.* **97** 083517
[24] Collins A T 1980 Vacancy enhanced aggregation of nitrogen in diamond *J. Phys. C: Solid State Phys.* **13** 2641–50
[25] Collins A T, Kanda H and Kitawaki H 2000 Colour changes produced in natural brown diamonds by high-pressure, high-temperature treatment *Diamond Relat. Mater.* **9** 113–22
[26] Watt G A, Newton M E and Baker J M 2001 EPR and optical imaging of the growth-sector dependence of radiation-damage defect production in synthetic diamond *Diamond Relat. Mater.* **10** 1681–3
[27] Goss J P, Briddon P R, Papagiannidis S and Jones R 2004 Interstitial nitrogen and its complexes in diamond *Phys. Rev.* B **70** 235208
[28] Woods G S and Collins A T 1982 The 1450 cm^{-1} infrared-absorption in annealed, electron-irradiated type-I diamonds *J. Phys. C: Solid State Phys.* **15** L949–52
[29] Burns R C, Cvetkovic V, Dodge C N, Evans D J F, Rooney M L T, Spear P M and Welbourn C M 1990 Growth-sector dependence of optical-features in large synthetic diamonds *J. Cryst. Growth* **104** 257–79

[30] Stroemann C V H, Tshisikhawe F, Hansen J O and Burns R C 2006 *International Patent Application* WO2006061672 (15/06/2006)
[31] Evans T and Qi Z 1982 The kinetics of the aggregation of nitrogen-atoms in diamond *Proc. R. Soc.* A **381** 159–78
[32] Evans T 1992 Aggregation of nitrogen in diamond *The Properties of Natural and Synthetic Diamond* ed J E Field (London: Academic) pp 259–90
[33] van Wyk J A, Reynhardt E C, High G L and Kiflawi I 1997 The dependences of ESR line widths and spin–spin relaxation times of single nitrogen defects on the concentration of nitrogen defects in diamond *J. Phys. D: Appl. Phys.* **30** 1790
[34] Smith W V, Sorokin P P, Gelles I L and Lasher G J 1959 Electron-spin resonance of nitrogen donors in diamond *Phys. Rev.* **115** 1546
[35] Lide David R 2006 *CRC Handbook of Chemistry and Physics* 87th edn (Boca Raton, FL: CRC Press)
[36] Collins A T and Dahwich A 2004 The annealing of interstitial-related optical centres in type Ib diamond *Diamond Relat. Mater.* **13** 1959–62
[37] Isoya J, Kanda H and Morita Y 1997 EPR identification of the $\langle 001 \rangle$-split $[\mathrm{B–N}]^{+}$ interstitialcy in diamond *Phys. Rev.* B **56** 6392